Vilnius
University
Press

Computations of local nonsimilar solutions for MHD flow of Reiner–Rivlin fluid

Sohail A. Khan[a] , **Tasawar Hayat** [a], **Ahmed Alsaedi** [b], **Shaher Momani** [c,d]

[a] Department of Mathematics, Quaid-I-Azam University,
Islamabad, 44000, Pakistan
sohailahmadkhan93@gmail.com

[b] Nonlinear Analysis and Applied Mathematics Research Group,
Faculty of Science, King Abdulaziz University,
P.O. Box 80207, Jeddah 21589, Saudi Arabia

[c] Department of Mathematics and Sciences,
College of Humanities and Sciences, Ajman University,
Ajman, United Arab Emirates

[d] Department of Mathematics, Faculty of Science,
University of Jordon, Amman 11942, Jordan

Abstract. Here local nonsimilar solution for hydromagnetic stretched flow of Reiner–Rivlin material is constructed. Heat generation, radiation, and dissipation in thermal expression are studied. Joule heating and chemical reaction of first order are under consideration. Entropy generation is computed. Nonlinear system is derived by adequate transformations. Optimal homotopy analysis technique computes the analysis. Attention is focused to achieve the results of concentration, fluid flow, entropy rate, and temperature. In addition, the skin friction, solutal transport rate and Nusselt number have been explained. Outcomes of magnetic field on velocity and entropy rate are found opposite. Large approximation of fluid parameter improves the fluid flow. Larger estimation of Brinkman number yields same results of entropy generation and temperature. Reduction in concentration is noted through Schmidt number. Higher reaction variable correspond to reduce concentration. Temperature and entropy generation through radiation variable has similar trend. Material variable has similar results for rate of mass transport and coefficient of skin friction. Radiation amplifies the thermal transport rate. Reverse effect for entropy rate and Bejan number is detected for magnetic field.

Keywords: thermal radiation, Reiner–Rivlin fluid, entropy generation, Joule heating.

1 Introduction

Non-Newtonian fluids are important for applications in industrial, biological, mechanical, and micromanufacturing engineering including oil exploration, drawing of plastic films, emulsions food processing, manufacturing of paints, petroleum industries, clay

coating, paper production, etc. [9, 31]. Existing literature ensures different models non-Newtonian fluids through their diverse characteristics. Reiner–Rivlin material [24, 25] is regarded to predict flow characteristics in various processes of geology and biology. Therefore Abdal et al. [1] studied bioconvective flow on this topic. Tabassum and Mustafa [27] examined heat transport in Reiner–Rivlin material. Flow by rotating disk is generated. Lv et al. [16] studied activation energy in Reiner–Rivlin nanomaterial flow subject to Cattaneo–Christov fluxes. Rashid and Mustafa [22] analyzed entropy optimized flow of Reiner–Rivlin material considering dissipation and radiation. Khan et al. [12] discussed features of homogeneous-heterogeneous reactions in magnetohydrodynamic Reiner–Rivlin liquid flow.

Magnetohydrodynamic (MHD) flows have received attention in view of industrial, physiological, and pharmaceutical processes such as energy conversion, magnetic resonance imaging (MRI), MHD thrusters, hyperthermia, plasma stability predictor, magnetic drug targeting, MHD generators, cancer therapy, etc. [26, 33, 34]. Radiation for magnetohydrodynamic nanoliquid flow by porous wall is studied in Amar and Kishan [2]. Kalpana et al. [11] addressed random and thermophoresis diffusions for hydromagnetic unsteady flow of nanoliquid in a wavy channel. Manzoor et al. [18] studied MHD flow by an oscillating porous wall. Ullah et al. [28] examined Ohmic heating for hydromagnetic flow of hybrid nanoliquid. Slip feature in MHD flow involving nanoliquid is considered by Vinita and Poply [30]. Madhu et al. [17] explored radiation in unsteady magnetized flow of Maxwell nanomaterial. Entropy for hydromagnetic dissipative flow of nanoliquid is examined in Govindaraju et al. [8]. MHD convective flow of nanomaterial in presence of heat generation is presented in Oudina et al. [19]. Yasir et al. [32] addressed radiative magnetohydrodynamic flow of hybrid nanomaterial.

Initially, Bejan [3, 4] estimated minimization procedure for studying thermodynamical system irreversibility in heat procedure with entropy production. Reedy et al. [23] discussed entropy for radiative flow of hydromagnetic Carreau fluid. Entropy generated flow of nanoliquid is presented in Buonomo et al. [6]. Hayat et al. [10] considered the entropy for modified Darcy–Forchheimer flow of Carreau liquid. Peristalsis in view of entropy generation and homogenous and heterogeneous reactions is examined by Vaidya et al. [29]. Chen [7] explored the irreversibility in rotating convective flow. Mondal and Mahapatra [20] examined thermal and solutal transportation analyses for convective nanomaterial flow with entropy rate inside a trapezoidal cavity.

It is noticed from existing information that entropy optimized flow of Reiner–Rivlin material is not much attention. Hence, the purpose of this communication is to model and simulate stretched flow on the title with radiation, heat generation, chemical reaction, and Ohmic heating. Chemically reactive flow with first order is taken. Adequate transformations are employed. Optimal homotopy analysis method (OHAM) leads to development of approximate solutions. The physical quantities under consideration are analyzed.

2   Modeling

MHD steady and stretched flow for Reiner–Rivlin material is explored. Radiation, Joule heating, heat generation, and entropy generation are present. Flow is subject to isothermal
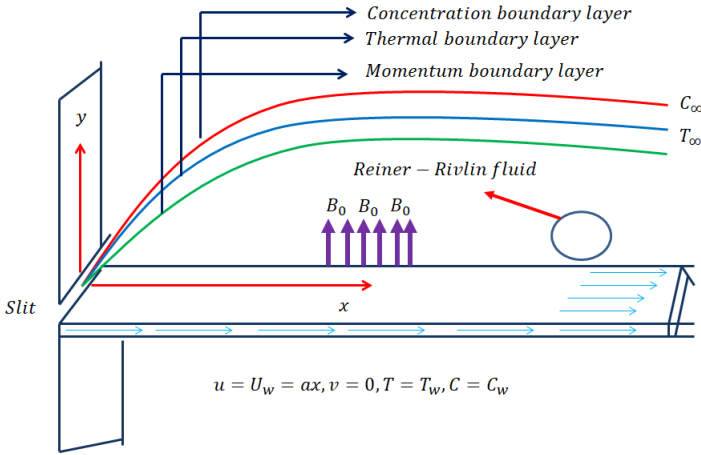
Figure 1. Flow sketch.

binary reaction. Magnetic field of strength B_0 is exerted. Absence of induced magnetic and electric fields are ensured. Stretching velocity is $u = u_w = ax$ ($u_w > 0$ being the stretching rate). Flow description is given in Fig. 1; see [13].

Boundary layer two-dimensional flow is governed by [13]

$$\frac{\partial u}{\partial x} + \frac{\partial v}{\partial y} = 0,$$

$$\rho\left(u\frac{\partial u}{\partial x} + v\frac{\partial u}{\partial y}\right) = \mu\frac{\partial^2 u}{\partial y^2} + 2\mu_c\left(\frac{\partial u}{\partial y}\frac{\partial^2 u}{\partial x \partial y} + \frac{\partial u}{\partial x}\frac{\partial^2 u}{\partial y^2}\right) - \sigma B_0^2 u,$$

$$u\frac{\partial T}{\partial x} + v\frac{\partial T}{\partial y}$$
$$= \frac{k}{\rho c_p}\left(1 + \frac{16\sigma^* T_\infty^3}{3kk^*}\right)\frac{\partial^2 T}{\partial y^2} + \frac{1}{\rho c_p}\left(\mu\left(\frac{\partial u}{\partial y}\right)^2 + 3\mu_c\left(\frac{\partial u}{\partial x} + \frac{\partial v}{\partial y}\right)\left(\frac{\partial u}{\partial y}\right)^2\right)$$
$$\quad + \frac{\sigma B_0^2}{\rho c_p}u^2 + \frac{Q_0}{\rho c_p}(T - T_\infty),$$

$$u\frac{\partial C}{\partial x} + v\frac{\partial C}{\partial y} = D_B\frac{\partial^2 C}{\partial y^2} - k_r(C - C_\infty)$$

with conditions [13]

$$u = u_w(x) = ax, \quad v = 0, \quad T = T_w, \quad C = C_w \quad \text{at } y = 0,$$
$$u \to 0, \quad T \to T_\infty, \quad C \to C_\infty \quad \text{as } y \to \infty.$$

In above expression, (x, y) indicates the Cartesian coordinates, ρ the density, (u, v) the velocity components, μ_c cross viscosity, σ the electrical conductivity, μ the dynamic viscosity, T the temperature, k the thermal conductivity, ν kinematic viscosity, T_w wall

temperature, Q_0 heat source coefficient, c_p specific heat, σ^* Stefan–Boltzman constant, T_∞ ambient temperature, C concentration, k^* the mean absorption coefficient, D_B mass diffusivity, C_w wall concentration, l reference length k_r reaction rate, and C_∞ ambient concentration.

Consider [13]

$$u = ax\frac{\partial f(\xi,\eta)}{\partial \eta}, \qquad v = -\sqrt{a\nu}f(\xi,\eta) - \sqrt{a\nu}\xi\frac{\partial f(\xi,\eta)}{\partial \xi},$$

$$\theta(\xi,\eta) = \frac{T - T_\infty}{T_w - T_\infty}, \qquad \phi(\xi,\eta) = \frac{C - C_\infty}{C_w - C_\infty},$$

$$\eta = \sqrt{\frac{a}{\nu}}\,y, \qquad \xi = \frac{x}{l}.$$

We have

$$\frac{\partial^3 f}{\partial \eta^3} + f\frac{\partial^2 f}{\partial \eta^2} + \xi\frac{\partial f}{\partial \xi}\frac{\partial^2 f}{\partial \eta^2} - \left(\frac{\partial f}{\partial \eta}\right)^2 - \xi\frac{\partial^2 f}{\partial \xi\partial \eta}\frac{\partial f}{\partial \eta}$$
$$+ 2K_1\left(\left(\frac{\partial^2 f}{\partial \eta^2}\right)^2 + \xi\frac{\partial^2 f}{\partial \eta^2}\frac{\partial^3 f}{\partial \xi\partial \eta^2} + \frac{\partial f}{\partial \eta}\frac{\partial^3 f}{\partial \eta^3} + \xi\frac{\partial^2 f}{\partial \xi\partial \eta}\frac{\partial^3 f}{\partial \eta^3}\right)$$
$$- M\frac{\partial f}{\partial \eta} = 0, \tag{1}$$

$$(1 + Rd)\frac{\partial^2 \theta}{\partial \eta^2} + Pr\,f\frac{\partial \theta}{\partial \eta} + Pr\xi\frac{\partial f}{\partial \xi}\frac{\partial \theta}{\partial \eta} - Pr\xi\frac{\partial f}{\partial \eta}\frac{\partial \theta}{\partial \xi}$$
$$+ Pr\,Ec\,\xi^2\left(\frac{\partial^2 f}{\partial \eta^2}\right)^2 + MPr\,Ec\,\xi^2\left(\frac{\partial f}{\partial \eta}\right)^2 + PrQ\theta = 0, \tag{2}$$

$$\frac{\partial^2 \phi}{\partial \eta^2} + Sc\,f\frac{\partial \phi}{\partial \eta} + Sc\,\xi\frac{\partial f}{\partial \xi}\frac{\partial \phi}{\partial \eta} - Sc\,\xi\frac{\partial \phi}{\partial \xi}\frac{\partial f}{\partial \eta} - Sc\,\gamma\phi = 0 \tag{3}$$

with

$$\frac{\partial f(\xi,0)}{\partial \eta} = 1, \qquad f(\xi,0) = -\xi\frac{\partial f(\xi,0)}{\partial \xi},$$

$$\theta(\xi,0) = 1, \qquad \phi(\xi,0) = 1, \tag{4}$$

$$\frac{\partial f(\xi,\infty)}{\partial \eta} = 0, \qquad \theta(\xi,\infty) = 0, \qquad \phi(\xi,\infty) = 0.$$

Here $K = \mu_c a/\mu$ denotes Reiner–Rivlin fluid parameter, $M = \sigma B_0^2/(a\rho)$ the magnetic variable, $Pr = \nu/\alpha$ the Prandtl number, $Rd = 16\sigma^* T_\infty^3/(3k^* k_f)$ the radiation variable, $Ec = a^2 l^2/(c_p(T_w - T_\infty))$ Eckert number, $Sc = \nu/D_B$ the Schmidt number, $Q = Q_0/(a\rho c_p)$ the heat generation variable, $Br = Pr\,Ec$ the Brinkman number, and $\gamma = k_r/a$ the reaction variable.

3 Quantities of interest

3.1 Skin friction coefficient

Its definition is

$$C_{fx} = \frac{\tau_{xy}|_{y=0}}{\rho u_w^2},$$

$$\tau_{xy} = \mu_f \left(\frac{\partial u}{\partial y} + \frac{\partial v}{\partial x} \right) + \mu_c \left(2\frac{\partial u}{\partial x} \left(\frac{\partial v}{\partial x} + \frac{\partial u}{\partial y} \right) + 2\frac{\partial v}{\partial y} \left(\frac{\partial v}{\partial x} + \frac{\partial u}{\partial y} \right) \right).$$

Nondimensional form is $C_{fx} Re_x^{1/2} = f''(0)$.

3.2 Nusselt number

Its definition is expressed by

$$Nu_x = \frac{x q_w}{k(T_w - T_\infty)}.$$

Here heat flux q_w satisfies

$$q_w = -\left(k + \frac{16\sigma^* T_\infty^3}{3k^*} \right) \left(\frac{\partial T}{\partial y} \right) \Big|_{y=0}.$$

Above two expressions lead to

$$Nu_x Re_x^{-1/2} = -(1 + Rd)\theta'(0)|_{\eta=0}.$$

3.3 Sherwood number

It is given by

$$Sh_x = \frac{x j_w}{D_B(C_w - C_\infty)}$$

in which mass flux j_w obeys

$$j_w = -D_B \left(\frac{\partial C}{\partial y} \right) \Big|_{y=0}.$$

Finally, one can get

$$Sh_x Re_x^{-1/2} = -\phi'(0).$$

4 Entropy generation

Its definition is

$$S_G = \frac{k}{T_\infty^2} \left(1 + \frac{16\sigma^* T_\infty^3}{3k^* k} \right) \left(\frac{\partial T}{\partial y} \right)^2 + \frac{1}{\rho c_p} \left(\mu \left(\frac{\partial u}{\partial y} \right)^2 + 3\mu_c \left(\frac{\partial u}{\partial x} + \frac{\partial v}{\partial y} \right) \left(\frac{\partial u}{\partial y} \right)^2 \right)$$

$$+ \frac{\sigma B_0^2}{T_\infty} u^2 + \frac{RD_B}{T_\infty} \frac{\partial T}{\partial y} \frac{\partial C}{\partial y} + \frac{RD_B}{C_\infty} \left(\frac{\partial C}{\partial y} \right)^2.$$

Above expression can be expressed as follows:

$$N_G(\xi, \eta) = \alpha_1(1 + Rd)\left(\frac{\partial \theta}{\partial \eta}\right)^2 + Br\xi^2\left(\frac{\partial^2 f}{\partial \eta^2}\right)^2 + MBr\xi^2\left(\frac{\partial f}{\partial \eta}\right)^2$$
$$+ L\frac{\partial \theta}{\partial \eta}\frac{\partial \phi}{\partial \eta} + L\frac{\alpha_2}{\alpha_1}\left(\frac{\partial \phi}{\partial \eta}\right)^2.$$

Here R characterizes the gas constant, $N_G = S_G \nu T_\infty/(ka(T_w - T_\infty))$ the entropy rate, $\alpha_1 = (T_w - T_\infty)/T_\infty$ heat ratio parameter, $L = RD_B(C_w - C_\infty)/k$ the diffusion parameter, $\alpha_2 = (C_w - C_\infty)/C_\infty$ the solutal ratio parameter, and Bejan number Be obeys

$$Be = \frac{\alpha_1(1 + Rd)(\frac{\partial \theta}{\partial \eta})^2 + L\frac{\partial \theta}{\partial \eta}\frac{\partial \phi}{\partial \eta} + L\frac{\alpha_2}{\alpha_1}\xi(\frac{\partial \phi}{\partial \eta})^2}{\alpha_1(1 + Rd)(\frac{\partial \theta}{\partial \eta})^2 + Br\xi^2(\frac{\partial^2 f}{\partial \eta^2})^2 + MBr\xi^2(\frac{\partial f}{\partial \eta})^2 + L\frac{\partial \theta}{\partial \eta}\frac{\partial \phi}{\partial \eta} + L\frac{\alpha_2}{\alpha_1}\xi(\frac{\partial \phi}{\partial \eta})^2}.$$

5 Solution methodology

5.1 Local-similar solution

We consider $\partial(\cdot)/\partial\xi = 0$ and $\partial(\cdot)/\partial\eta$ for prime regarding such solutions through Eqs. (1)–(4) and obtain

$$f''' + ff'' - f'^2 + 2K(f''^2 + f'f''') - Mf' = 0,$$
$$(1 + Rd)\theta'' + Pr f\theta' + Pr Ec\xi^2 f''^2 + MPr Ec\xi^2 f'^2 + PrQ\theta = 0,$$
$$\phi'' + Sc f\phi' - Sc\gamma\phi = 0$$

with

$$f'(\xi, 0) = 1, \qquad f(\xi, 0) = 0, \qquad \theta(\xi, 0) = 1, \qquad \phi(\xi, 0) = 1,$$
$$f'(\xi, \infty) = 0, \qquad \theta(\xi, \infty) = 0, \qquad \phi(\xi, \infty) = 0.$$

5.2 Local nonsimilar solution

For local nonsimilar solutions, we consider $\partial f/\partial\xi = p$, $\partial^2 f/\partial\xi\partial\eta = \partial f'/\partial\xi = p'$, $\partial\theta/\partial\xi = q$, $\partial^2\theta/\partial\xi\partial\eta = \partial\theta'/\partial\xi = q'$, $\partial\phi/\partial\xi = g$, $\partial^2\phi/\partial\xi\partial\eta = \partial\phi'/\partial\xi = g'$. Denoting $\partial(\cdot)/\partial\eta$ by prime in Eqs. (1)–(4), we thus have

$$f''' + ff'' - f'^2 + \xi pf'' - \xi p'f' + 2K(f''^2 + \xi p''f'' + f'f''' + \xi p'f''') - Mf' = 0,$$
$$(1 + Rd)\theta'' + Pr f\theta' - Pr\xi q\theta' + Pr\xi pf' + MPr Ec\xi^2 f'^2 + PrQ\theta = 0,$$
$$\phi'' + Sc f\phi' + Sc\xi p\phi' - Sc\xi gf' - Sc\gamma\phi = 0$$

with

$$f'(\xi, 0) = 1, \qquad f(\xi, 0) = -\xi p(\xi, 0), \qquad \theta(\xi, 0) = 1, \qquad \phi(\xi, 0) = 1,$$
$$f'(\xi, \infty) = 0, \qquad \theta(\xi, \infty) = 0, \qquad \phi(\xi, \infty) = 0.$$

Taking differentiation (w.r.t. ξ) of above expressions and neglecting the terms containing $\partial p(\xi, \eta)/\partial \xi$, $\partial^2 p(\xi, \eta)/\partial \eta \partial \xi$, $\partial q(\xi, \eta)/\partial \xi$, $\partial^2 q(\xi, \eta)/\partial \eta \partial \xi$, $\partial h(\xi, \eta)/\partial \xi$, $\partial^2 h(\xi, \eta)/\partial \eta \partial \xi$, $\partial g(\xi, \eta)/\partial \xi$ and $\partial^2 g(\xi, \eta), \partial \eta \partial \xi$, we get

$$p''' + 2pf'' + fp'' + \xi pp'' - 3p'f' - \xi p'^2 - Mp'$$
$$2K \left(3f''p'' + \xi p''^2 + 2p'f''' + f'p''' + \xi p'p''' \right) = 0,$$
$$(1 + Rd)q'' + 2Pr p\theta' + Pr fq' + Pr \xi pq' - Pr f'q - Pr \xi p'q + Pr Qq$$
$$+ 2MPr Ec \left(\xi f'^2 + \xi^2 p'f' \right) + 2Pr Ec \left(\xi f''^2 + \xi^2 p''f'' \right) = 0,$$
$$g'' + 2Sc p\phi' + Sc fg' + Sc \xi pg' - Sc gf' - Sc \xi gp' - Sc \gamma g = 0$$

with

$$p'(\xi, 0) = 0, \qquad p(\xi, 0) = 0, \qquad q(\xi, 0) = 0, \qquad g(\xi, 0) = 0,$$
$$p'(\xi, \infty) = 0, \qquad q(\xi, \infty) = 0, \qquad g(\xi, \infty) = 0.$$

The linear operators and initial approximations required for OHAM [14, 15] solutions are

$$f_0(\eta) = 1 - \mathrm{e}^{-\eta}, \qquad \theta_0(\eta) = \mathrm{e}^{-\eta}, \qquad \phi_0(\eta) = \mathrm{e}^{-\eta},$$
$$L_f = \frac{\partial^3}{\partial \eta^3} - \frac{\partial}{\partial \eta}, \qquad L_\theta = \frac{\partial^2}{\partial \eta^2} - 1, \qquad L_\phi = \frac{\partial^2}{\partial \eta^2} - 1$$

with

$$L_f \left[a_0 + a_1 \mathrm{e}^{-\eta} + a_2 \mathrm{e}^{\eta} \right], \qquad L_\theta \left[a_3 \mathrm{e}^{-\eta} + a_4 \mathrm{e}^{\eta} \right],$$
$$L_\phi \left[a_5 \mathrm{e}^{-\eta} + a_6 \mathrm{e}^{\eta} \right].$$

Here a_i, $i = 0, 1, 2, \ldots, 6$, signify arbitrary constants, $\hbar_f$, $\hbar_\theta$, and $\hbar_\phi$ are auxiliary variables, and $p^* \in [0, 1]$ indicates an embedding parameter.

5.3 Zeroth-order deformation problem

We have

$$(1 - p^*)L_f \left[f(\eta; p^*) - f_0(\eta) \right] = p^* \hbar_f \aleph_f \left[f(\eta; p^*) \right],$$
$$(1 - p^*)L_\theta \left[\theta(\eta; p^*) - \theta_0(\eta) \right] = p^* \hbar_\theta \aleph_\theta \left[\theta(\eta; p^*) \right],$$
$$(1 - p^*)L_\phi \left[\phi(\eta; p^*) - \phi_0(\eta) \right] = p^* \hbar_\phi \aleph_\phi \left[\phi(\eta; p^*) \right]$$

with

$$f'(0, p^*) = 1, \qquad f(0, p^*) = 0, \qquad \theta(0, p^*) = 1, \qquad \phi(0, p^*) = 0,$$
$$f'(\infty, p^*) = 0, \qquad \theta(\infty, p^*) = 0, \qquad \phi(\infty, p^*) = 0,$$

$$\aleph_f\big[f(\eta;p^*)\big] = \frac{\partial^3 f(\eta;p^*)}{\partial\eta^3} + f(\eta;p^*)\frac{\partial^2 f(\eta;p^*)}{\partial\eta^2} - \left(\frac{\partial f(\eta;p^*)}{\partial\eta}\right)^2$$

$$- M\frac{\partial f(\eta;p^*)}{\partial\eta} + 2K\left(\left(\frac{\partial^2 f(\eta;p^*)}{\partial\eta^2}\right)^2 + \frac{\partial f(\eta;p^*)}{\partial\eta}\frac{\partial^3 f(\eta;p^*)}{\partial\eta^3}\right),$$

$$\aleph_\theta\big[\theta(\eta;p^*)\big] = (1+Rd)\frac{\partial^2\theta(\eta;p^*)}{\partial\eta^2} + Pr\,f(\eta;p^*)\frac{\partial\theta(\eta;p^*)}{\partial\eta}$$

$$+ M\,Pr\,Ec\,\xi^2\left(\frac{\partial f(\eta;p^*)}{\partial\eta}\right)^2 + Pr\,Ec\,\xi^2\left(\frac{\partial^2 f(\eta;p^*)}{\partial\eta^2}\right)^2$$

$$+ Pr\,Q\theta(\eta;p^*),$$

$$\aleph_\phi\big[\phi(\eta;p^*)\big] = \frac{\partial^2\phi(\eta;p^*)}{\partial\eta^2} + Sc\,f(\eta;p^*)\frac{\partial\phi(\eta;p^*)}{\partial\eta} - Sc\,\gamma\phi(\eta;p^*).$$

5.4 Problems at mth order

$$L_f\big[f_m(\eta) - \chi_m f_{m-1}(\eta)\big] = \hbar_f Re_m^f(\eta),$$

$$L_\theta\big[\theta_m(\eta) - \chi_m\theta_{m-1}(\eta)\big] = \hbar_\theta Re_m^\theta(\eta),$$

$$L_\phi\big[\phi_m(\eta) - \chi_m\phi_{m-1}(\eta) = \hbar_\phi Re_m^\phi(\eta),$$

$$\frac{\partial f(\eta;p^*)}{\partial\eta}\bigg|_{\eta=0} = f(\eta;p^*)|_{\eta=0} = \frac{\partial f(\eta;p^*)}{\partial\eta}\bigg|_{\eta=\infty} = 0,$$

$$\theta(\eta;p^*)|_{\eta=0} = \theta(\eta;p^*)|_{\eta=\infty} = 0, \qquad \phi(\eta;p^*)|_{\eta=0} = \phi(\eta;p^*)|_{\eta=\infty} = 0,$$

$$Re_m^f(\eta) = f_{m-1}''' + \sum_{k=0}^{m-1} f_{m-1-k}f_k'' - \sum_{k=0}^{m-1} f_{m-1-k}'f_k' - Mf_{m-1}'$$

$$+ 2K\left(\sum_{k=0}^{m-1} f_{m-1-k}''f_k'' + \sum_{k=0}^{m-1} f_{m-1-k}'f_k'''\right),$$

$$Re_m^\theta(\eta) = (1+Rd)\theta_{m-1}'' + Pr\sum_{k=0}^{m-1} f_{m-1-k}\theta_k' + Pr\,Ec\,\xi^2\sum_{k=0}^{m-1} f_{m-1-k}''f_k''$$

$$+ M\,Pr\,Ec^2\sum_{k=0}^{m-1} f_{m-1-k}'f_k' + Pr\,Q\theta_{m-1},$$

$$Re_m^\phi(\eta) = \phi_{m-1}'' + Sc\sum_{k=0}^{m-1} f_{m-1-k}\phi_k' - Sc\,\gamma\phi_{m-1},$$

where

$$\chi_m = \begin{cases} 0, & m \leqslant 0, \\ 1, & m > 0. \end{cases}$$

6 Convergence

Initially, OHAM is given by Liao [14, 15]. The mathematical expressions for OHAM are given as

$$
\epsilon_m^f = \frac{1}{K+1} \sum_{i=0}^{K} \left[\aleph_f \left(\sum_{j=0}^{m} f(\eta) \right)_{\eta=i\delta^*\eta} \right]^2,
$$

$$
\epsilon_m^\theta = \frac{1}{K+1} \sum_{i=0}^{K} \left[\aleph_\theta \left(\sum_{j=0}^{m} f(\eta), \sum_{j=0}^{m} \theta(\eta) \right)_{\eta=i\delta^*\eta} \right]^2,
$$

$$
\epsilon_m^\phi = \frac{1}{K+1} \sum_{i=0}^{K} \left[\aleph_\phi \left(\sum_{j=0}^{m} f(\eta), \sum_{j=0}^{m} \theta(\eta), \sum_{j=0}^{m} \phi(\eta) \right)_{\eta=i\delta^*\eta} \right]^2.
$$

Total residual error is given by [15]

$$
\epsilon_m^t = \epsilon_m^f + \epsilon_m^\theta + \epsilon_m^\phi.
$$

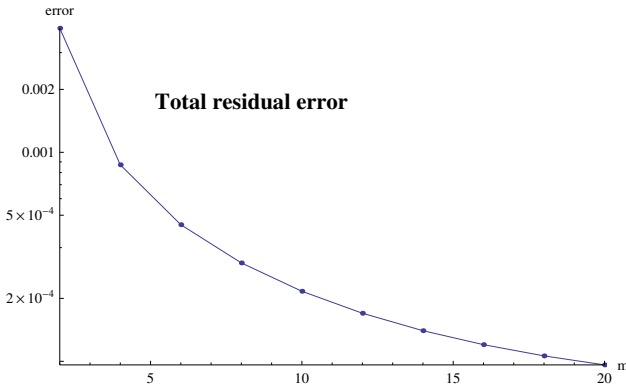The total and individual averaged squared error have been given through Fig. 2 and Table 1.

Figure 2. Total residual error.

Table 1. Averaged squared residual errors individually.

m	ε_f^m	ε_θ^m	ε_ϕ^m
2	0.000129351	0.00268208	0.00111362
6	$1.31098 \cdot 10^{-6}$	0.000380502	0.0000686456
10	$3.00317 \cdot 10^{-8}$	0.000198497	0.0000178514
14	$6.86171 \cdot 10^{-10}$	0.000134067	$6.05838 \cdot 10^{-6}$
18	$2.46517 \cdot 10^{-11}$	0.000103795	$2.37013 \cdot 10^{-6}$
20	$4.85944 \cdot 10^{-12}$	0.0000945817	$1.53811 \cdot 10^{-6}$

7   Comparison of results

Table 2 is prepared for comparison with analysis of studies [5, 21]. The results agree in reasonable agreement.

Table 2. Comparative study for Nusselt number Nu_x.

	Pr	1.0	2.0	3.0
Bidin and Nazar [5]	Keller-box method	0.9547	1.4714	1.8961
Mukhopadhyay [21]	Shooting method	0.9547	1.4714	1.8961
Present results	OHAM method	0.954563	1.471035	1.896953

8   Graphical analysis

This section arranges discussion for velocity, concentration, thermal field, Nusselt number, entropy rate, and Sherwood number.

8.1   Velocity

Fig. 3 describes magnetic field effect on $f'(\eta)$. Physically, higher M leads to amplify resistive force. As a result, the decay in velocity is guaranteed. Fig. 4 certifies the role of Reiner–Rivlin fluid parameter on velocity. Clearly, the velocity amplified for larger Reiner–Rivlin fluid variable. Physically, larger estimation of K_1 corresponds to viscous force decay. Ultimately, the velocity is enhanced.

8.2   Temperature

Fig. 5 portrays the influence of temperature for radiation. Physically, higher radiation leads to decay of the mean absorption coefficient. This effectively transfers more heat to the fluid. As a result, temperature is boosted. Influence of heat generation variable upon temperature is sketched through Fig. 6. Larger approximation of heat generation variable corresponds to an increase in temperature. Fig. 7 elucidates the influence of Br on
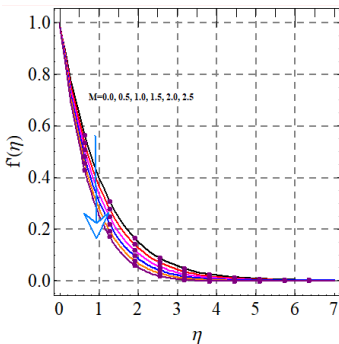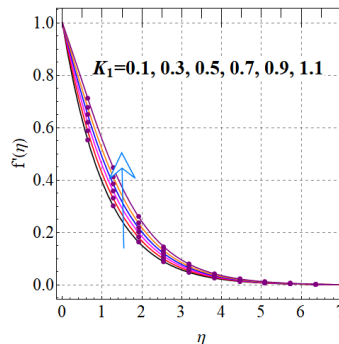

Figure 3. $f'(\eta)$ against M.
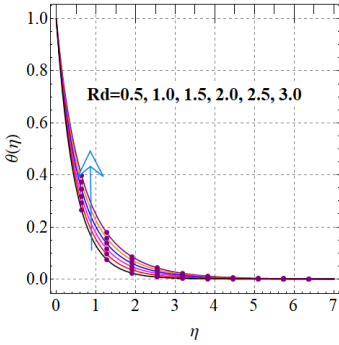
Figure 4. $f'(\eta)$ against K_1.

Figure 5. $\theta(\eta)$ versus Rd.
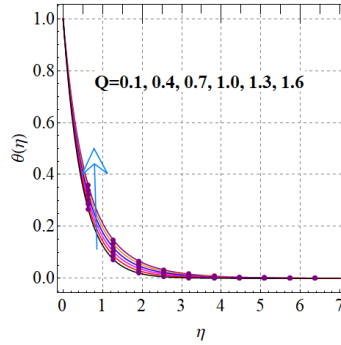
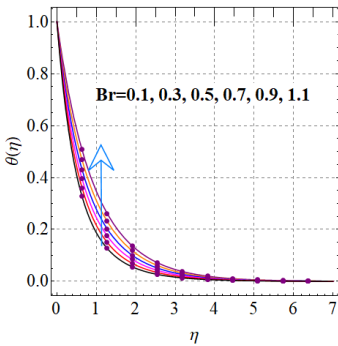

Figure 6. $\theta(\eta)$ versus Q.

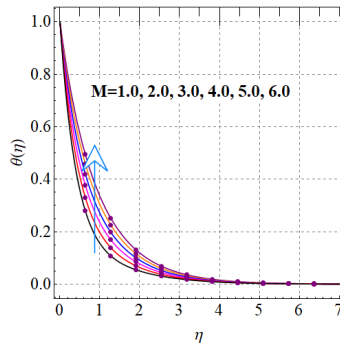**Figure 7.** $\theta(\eta)$ versus Br.

Figure 8. $\theta(\eta)$ versus M.

temperature. Physically, higher estimation of Brinkman number corresponds to enhancement of kinetic energy in fluid flow system. Thermal field is augmented. Fig. 8 is developed in order to recognize the temperature against M. Clearly, higher M rises the Lorentz force in which collisions among the fluid particles increase and thermal field is boosted.

8.3 Concentration

Fig. 9 depicts variation of $(\phi(\eta))$ for γ. Physically, higher γ corresponds to enhancement of solute molecules chemical reaction. As a result, concentration decay is guaranteed. Fig. 10 is sketched to show Sc outcome for concentration. Higher Sc decay mass diffusivity, and therefore $\phi(\eta)$ diminished.

8.4 Entropy generation

Consequence of magnetic variable upon entropy rate $N_G(\eta)$ is exposed in Fig. 11. Clearly, the larger M, the more resistive force. It yields disorder in system and so an increase for entropy rate occurs. Inspection of entropy generation in view of radiation Rd is evaluated in Fig. 12. Physically, higher radiation reduces the mean absorption coefficient. Disorder
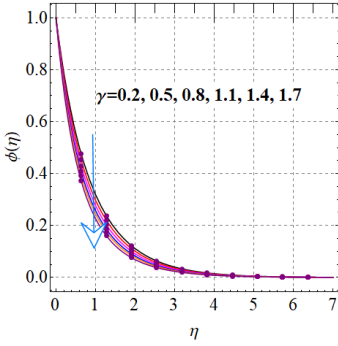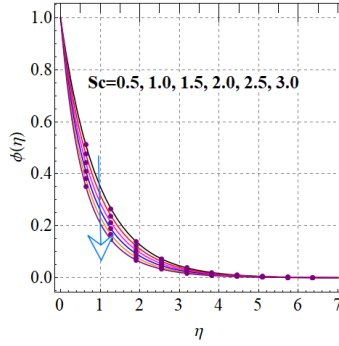
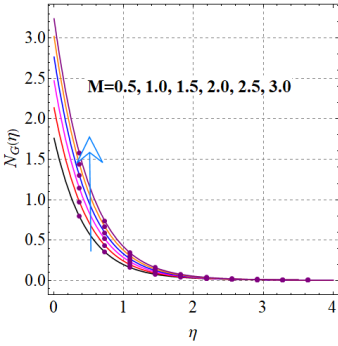**Figure 9.** $\phi(\eta)$ against γ.

Figure 10. $\phi(\eta)$ against Sc.

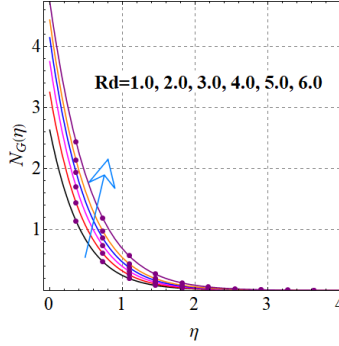**Figure 11.** $N_G(\eta)$ agaisnt M.

Figure 12. $N_G(\eta)$ agaisnt Rd.

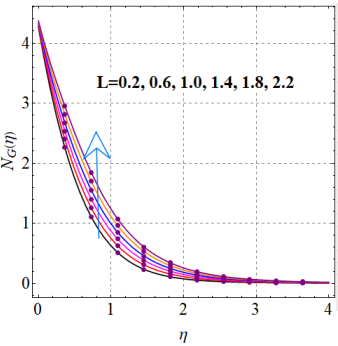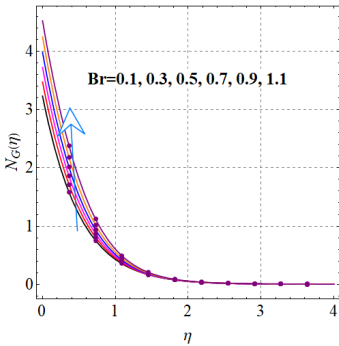**Figure 13.** $N_G(\eta)$ agaisnt L.

Figure 14. $N_G(\eta)$ agaisnt Br.

in system increases, and entropy generation enhances. Fig. 13 explains that increasing values of diffusion parameter boost up the entropy optimization. Outcome of Br on entropy rate is portrayed in Fig. 14. Viscous force is enhanced through higher Br. Disorder in system enhanced, and thus entropy generation increased.
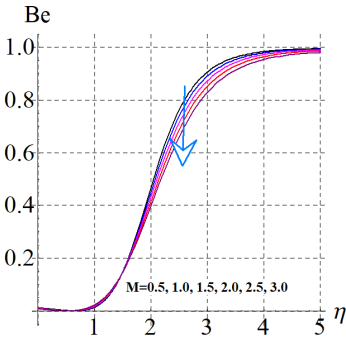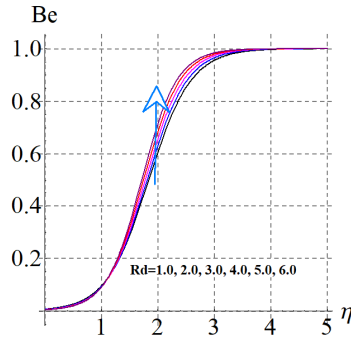
Figure 15. *Be* against *M*.

Figure 16. *Be* against *Rd*.
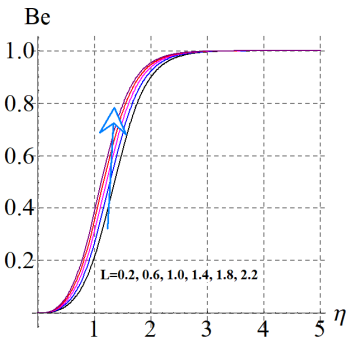
Figure 17. *Be* against *L*.
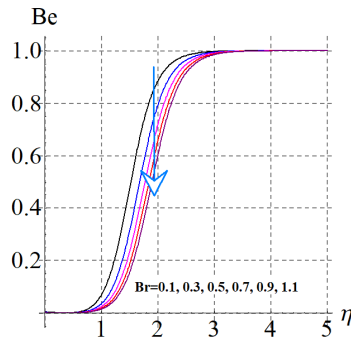
Figure 18. *Be* against *Br*.

8.5   Bejan number

Fig. 15 describes magnetic variable impact on Be. Larger approximation of magnetic field reduces Be. Fig. 16 shows influence for Be against radiation variable. Physically, higher radiation variable gives the rise to Be. An augmentation of Bejan number occurs against diffusion parameter; see Fig. 17. Fig. 18 certifies the role of Br on Bejan number. Here one can find that Bejan number decreased for larger Brinkman Br number.

8.6   Interesting quantities

Tables 3–5 comprise physical features of influential variables on physical quantities $C_{fx}Re_x^{1/2}$, $Nu_x Re_x^{-1/2}$, $Sh_x Re_x^{-1/2}$.

8.6.1   Rate of skin friction

Table 3 is designed to show the influence of K and M on $C_{fx}Re_x^{1/2}$. Clearly, $C_{fx}Re_x^{1/2}$ decays through the fluid parameter K. An improvement in the velocity gradient $C_{fx}Re_x^{1/2}$ is seen for the magnetic variable M.

Table 3. Skin friction rate results.

k	M	$C_{fx}Re_x^{1/2}$
0.1	0.5	0.935649
0.4		0.732758
0.7		0.620501
1.0		0.547243
0.1	0.5	1.09056
	1.0	1.25795
	1.5	1.40562
	2.0	1.53920

Table 4. Thermal transport rate results.

Rd	M	Q	$Nu_x Re_x^{-1/2}$
0.5	0.5	0.1	1.86434
1.0			2.34658
2.5			2.69795
3.5			2.97359
1.0	0.5	0.1	1.51156
	1.0		1.69384
	1.5		1.89645
	2.0		2.12750
0.1	0.5	0.2	1.80955
		0.5	1.44613
		0.8	1.01468
		1.1	0.468457

Table 5. Mass transport rate results.

K	Sc	γ	$Sh_x Re_x^{-1/2}$
0.2	0.5	0.5	0.643443
0.4			0.650780
0.6			0.656835
0.8			0.666315
0.1	0.5	0.5	0.628797
	1.5		0.921151
	1.5		1.15058
	2.0		1.34559
0.1	0.5	0.1	0.425860
		0.4	0.584966
		0.7	0.778285
		1.3	0.901772

8.6.2   *Rate of heat transfer*

The value of the expression $Nu_x Re_x^{-1/2}$ for emerging variables is organized in Table 4. Here an increasing behavior of $Nu_x Re_x^{-1/2}$ for Rd and M is noticed. Further, the heat transport rate acts as decaying function of heat generation variable.

8.6.3   *Rate of mass transfer*

The analysis of $Sh_x Re_x^{-1/2}$ is organized through Table 5. Clearly, it is found that higher reaction variable γ enhances $Sh_x Re_x^{-1/2}$. A reverse impact holds for gradient of concentration through Schmidt number and Reiner–Rivlin fluid variable.

9   Conclusions

Main points of present study are included below.

- Intensifying Reiner–Rivlin liquid variable leads to amplify the velocity, while reverse impact holds for Sherwood number.
- Velocity field declines for higher magnetic variable.
- Influences of heat generation and radiation on thermal field are similar.
- Temperature and entropy rate are qualitatively similar for Brinkman number.
- Concentration declines for reaction variable.

- Higher Schmidt number leads to decay of concentration.
- Amplified version of radiation intensifies entropy optimization.
- Entropy generation enlarges with diffusion variable enhancement.
- Similar characteristics for drag force and mass transport rate are detected for liquid parameter.
- Nusselt number through radiation is enhanced.
- Bejan number and entropy rate through magnetic field are enhanced.

References

1. S. Abdal, A. Mariam, B. Ali, S. Younas, L. Ali, D. Habib, Implications of bioconvection and activation energy on Reiner–Rivlin nanofluid transportation over a disk in rotation with partial slip, *Chin. J. Phys., Taipei*, **73**:672–683, 2021, `https://doi.org/10.1016/j.cjph.2021.07.022`.

2. N. Amar, N. Kishan, The influence of radiation on MHD boundary layer flow past a nano fluid wedge embedded in porous media, *Partial Differ. Equations Appl. Math.*, **4**:100082, 2021, `https://doi.org/10.1016/j.padiff.2021.100082`.

3. A. Bejan, Second law analysis in heat transfer, *Energy*, **5**(8–9):720–732, 1980, `https://doi.org/10.1016/0360-5442(80)90091-2`.

4. A. Bejan, The equivalence of maximum power and minimum entropy generation rate in the optimization of power plants, *J. Energy Res. Technol.*, **182**(2):98–101, 1996, `https://doi.org/10.1115/1.2792711`.

5. B. Bidin, R. Nazar, Numerical solution of the boundary layer flow over an exponentially stretching sheet with thermal radiation, *European Journal of Scientific Research*, **33**(4):710–717, 2009.

6. B. Buonomo, A. di Pasqua, O. Manca, S. Nappo, S. Nardini, Entropy generation analysis of laminar forced convection with nanofluids at pore length scale in porous structures with Kelvin cells, *Int. Commun. Heat Mass Transfer*, **132**:105883, 2022, `https://doi.org/10.1016/j.icheatmasstransfer.2022.105883`.

7. S. Chen, Entropy generation inside disk driven rotating convectional flow, *Int. J. Therm. Sci.*, **50**(4):626–638, 2011, `https://doi.org/10.1016/j.ijthermalsci.2010.11.012`.

8. M. Govindaraju, N.V. Ganesh, B. Ganga, A.K. Abdul Hakeem, Entropy generation analysis of magneto hydrodynamic flow of a nanofluid over a stretching sheet, *J. Egypt. Math. Soc.*, **23**(2):429–434, 2015, `https://doi.org/10.1016/j.joems.2014.04.005`.

9. T. Han, S. Zhang, C. Zhang, Unlocking the secrets behind liquid superlubricity: A state-of-the-art review on phenomena and mechanisms, *Friction*, **10**(8):1137–1165, 2022, `https://doi.org/10.1007/s40544-021-0586-1`.

10. T. Hayat, F. Haider, A. Alsaedi, B. Ahmad, Entropy generation analysis of Carreau fluid with entire new concepts of modified Darcy's law and variable characteristics, *Int. Commun. Heat Mass Transfer*, **120**:105073, 2021, `https://doi.org/10.1016/j.icheatmasstransfer.2020.105073`.

11. G. Kalpana, K.R. Madhura, Ramesh B. Kudenatti, Numerical study on the combined effects of Brownian motion and thermophoresis on an unsteady magnetohydrodynamics nanofluid boundary layer flow, *Math. Comput. Simul.*, **200**:78–96, 2022, `https://doi.org/` `https://doi.org/10.1016/j.matcom.2022.04.010`.

12. S.A. Khan, T. Hayat, A. Alsaedi, Irreversibility analysis in hydromagnetic Reiner-Rivlin nanofluid with quartic autocatalytic chemical reactions, *Int. Commun. Heat Mass Transfer*, **130**:105797, 2022, `https://doi.org/10.1016/j.icheatmasstransfer.` `2021.105797`.

13. S.A. Khan, T. Hayat, A. Alsaedi, Simultaneous features of Soret and Dufour in entropy optimized flow of Reiner-Rivlin fluid considering thermal radiation, *Int. Commun. Heat Mass Transfer*, **137**:106297, 2022, `https://doi.org/10.1016/j.` `icheatmasstransfer.2022.106297`.

14. N. Kousar, S. Liao, Series solution of non-similarity boundary-layer flows over a porous wedge, *Transp. Porous Med.*, **83**:397–412, 2010, `https://doi.org/10.1007/s11242-009-` `9450-x`.

15. S. Liao, An optimal homotopy-analysis approach for strongly nonlinear differential equations, *Commun. Nonlinear Sci. Numer. Simul.*, **15**(8):2003–2016, 2010, `https://doi.org/10.` `1016/j.cnsns.2009.09.002`.

16. Yu-Pei Lv, Hina Gul, Muhammad Ramzan, Jae Dong Chung, Muhammad Bilal, Bioconvective Reiner–Rivlin nanofluid flow over a rotating disk with Cattaneo–Christov flow heat flux and entropy generation analysis, *Sci. Rep.*, **11**(1):15859, 2021, `https://doi.org/10.1038/` `s41598-021-95448-y`.

17. M. Madhu, N. Kishan, A.J. Chamkha, Unsteady flow of a Maxwell nanofluid over a stretching surface in the presence of magnetohydrodynamic and thermal radiation effects, *Propul. Power Res.*, **6**(1):31–40, 2017, `https://doi.org/10.1016/j.jppr.2017.01.002`.

18. T. Manzoor, K. Nazar, S. Iqbal, H.U. Manzoor, Theoretical investigation of unsteady MHD flow within non-stationary porous plates, *Heliyon*, **7**(3), 2021, `https://doi.org/10.` `1016/j.heliyon.2021.e06567`.

19. F. Mebarek-Oudina, A. Aissa, B. Mahanthesh, H.F. Öztop, Heat transport of magnetized newtonian nanoliquids in an annular space between porous vertical cylinders with discrete heat source, *Int. Commun. Heat Mass Transfer*, **117**:104737, 2020, `https://doi.org/10.` `1016/j.icheatmasstransfer.2020.104737`.

20. P. Mondal, T.R. Mahapatra, MHD double-diffusive mixed convection and entropy generation of nanofluid in a trapezoidal cavity, *Int. J. Mech. Sci.*, **208**:106665, 2021, `https://doi.` `org/10.1016/j.ijmecsci.2021.106665`.

21. S. Mukhopadhyay, MHD boundary layer flow and heat transfer over an exponentially stretching sheet embedded in a thermally stratified medium, *Alexandria Eng. J.*, **52**(3):259–265, 2013, `https://doi.org/10.1016/j.aej.2013.02.003`.

22. M.U. Rashid, M. Mustafa, A study of heat transfer and entropy generation in von Kármán flow of Reiner-Rivlin fluid due to a stretchable disk, *Ain Shams Engineering Journal*, **12**(1):875–883, 2021, `https://doi.org/10.1016/j.asej.2020.06.017`.

23. C.S. Reedy, P. Srihari, F. Ali, K. Naikoti, Numerical analysis of Carreau fluid flow over a vertical porous microchannel with entropy generation, *Partial Differ. Equations Appl. Math.*, **5**:100304, 2022, `https://doi.org/10.1016/j.padiff.2022.100304`.

24. M. Reiner, A mathematical theory of dilatancy, *Am. J. Math.*, **67**(3):350–362, 1945, `https://doi.org/10.2307/2371950`.

25. R.S. Rivlin, The hydrodynamics of non-Newtonian fluids. I, *Proc. R. Soc. Lond., Ser. A*, **193**(1033):260–281, 1948, `https://doi.org/10.1098/rspa.1948.0044`.

26. L. Sun, G. Wang, C. Zhang, Experimental investigation of a novel high performance multi-walled carbon nano-polyvinylpyrrolidone/silicon-based shear thickening fluid damper, *J. Intell. Mater. Syst. Struct.*, **35**(6):661–672, 2024, `https://doi.org/10.1177/1045389X2312229`.

27. M. Tabassum, M. Mustafa, A numerical treatment for partial slip flow and heat transfer of non-Newtonian Reiner-Rivlin fluid due to rotating disk, *International Journal of Heat and Mass Transfer*, **123**:979–987, 2018, `https://doi.org/10.1016/j.ijheatmasstransfer.2018.03.040`.

28. H. Ullah, T. Hayat, S. Ahmad, M.Sh. Alhodaly, Sh. Momani, Numerical simulation of MHD hybrid nanofluid flow by a stretchable surface, *Chin. J. Phys., Taipei*, **71**:597–609, 2021, `https://doi.org/10.1016/j.cjph.2021.03.017`.

29. H. Vaidya, C. Rajashekhar, G. Manjunatha, A. Wakif, K.V. Prasad, I.L. Animasaun, K. Shivaraya, Analysis of entropy generation and biomechanical investigation of MHD Jeffery fluid through a vertical non-uniform channel, *Case Stud. Therm. Eng.*, **28**:101538, 2021, `https://doi.org/10.1016/j.csite.2021.101538`.

30. V. Vinita, V. Poply, Impact of outer velocity MHD slip flow and heat transfer of nanofluid past a stretching cylinder, *Materials Today: Proceedings*, **26**:3429–3435, 2020, `https://doi.org/10.1016/j.matpr.2019.11.304`.

31. D. Xiao, L. Chen, X. Xu, G. Tang, Y. Hu, B. Guo, M. Liu, C. Yuan, G. Li, Coupling model of wellbore heat transfer and cuttings bed height during horizontal well drilling, *Phys. Fluids*, **36**(9):097163, 2024, `https://doi.org/10.1063/5.0222401`.

32. M. Yasir, A. Ahmed, M. Khan, Carbon nanotubes based fluid flow past a moving thin needle examine through dual solutions: Stability analysis, *J. Energy Storage*, **48**:103913, 2022, `https://doi.org/10.1016/j.est.2021.103913`.

33. S. Zeng, J. Liu, C. Ma, Topology optimization in cooling moving heat sources for enhanced precision of machine tool feed drive systems, *Int. J. Therm. Sci.*, **202**:109065, 2024, `https://doi.org/10.1016/j.ijthermalsci.2024.109065`.

34. W. Zhou, C. Ma, L. Yang, F. Luo, J. Liu, Regulation of thermo-fluid-solid coupling characteristics in high-speed spindle-bearing system for boring machine tool based on sintered-core heat pipes, *Int. Commun. Heat Mass Transfer*, **157**:107717, 2024, `https://doi.org/10.1016/j.icheatmasstransfer.2024.107717`.